

# Updated global fit to three neutrino mixing: status of the hints of $\theta_{13} > 0$

---

## M. C. Gonzalez-Garcia

*C.N. Yang Institute for Theoretical Physics  
State University of New York at Stony Brook  
Stony Brook, NY 11794-3840, USA,*  
and: *Institució Catalana de Recerca i Estudis Avançats (ICREA),  
Departament d'Estructura i Constituents de la Matèria and Institut de Ciències del  
Cosmos, Universitat de Barcelona, Diagonal 647, E-08028 Barcelona, Spain*  
*E-mail: concha@insti.physics.sunysb.edu*

## Michele Maltoni

*Instituto de Física Teórica UAM/CSIC, Facultad de Ciencias, Universidad Autónoma  
de Madrid, Cantoblanco, E-28049 Madrid, Spain*  
*E-mail: michele.maltoni@uam.es*

## Jordi Salvado

*Departament d'Estructura i Constituents de la Matèria and Institut de Ciències del  
Cosmos, Universitat de Barcelona, 647 Diagonal, E-08028 Barcelona, Spain*  
*E-mail: jsalvado@ecm.ub.es*

**ABSTRACT:** We present an up-to-date global analysis of solar, atmospheric, reactor and accelerator neutrino data in the framework of three-neutrino oscillations. We discuss in detail the statistical significance of the observed “hint” of non-zero  $\theta_{13}$  in the solar sector at the light of the latest experimental advances, such as the Borexino spectral data, the lower value of Gallium rate recently measured in SAGE, and the low energy threshold analysis of the combined SNO phase I and phase II. We also study the robustness of the results under changes of the inputs such as the choice of solar model fluxes and a possible modification of the Gallium capture cross-section as proposed by SAGE. In the atmospheric sector we focus on the latest results for  $\nu_e$  appearance from MINOS and on the recent Super-Kamiokande results from the combined phases I, II and III, and we discuss their impact on the determination of  $\theta_{13}$ . Finally, we combine all the data into a global analysis and determine the presently allowed ranges of masses and mixing.

**KEYWORDS:** neutrino oscillations, solar and atmospheric neutrinos.

---

## Contents

<b>1. Introduction</b>	<b>1</b>
<b>2. Leading <math>\Delta m_{21}^2</math> oscillations: solar and KamLAND data</b>	<b>2</b>
2.1 Impact of $\theta_{13}$ on the solar analysis	5
2.2 Combination with KamLAND and the hint of $\theta_{13} \neq 0$	9
<b>3. Leading <math>\Delta m_{31}^2</math> oscillations: atmospheric, CHOOZ and accelerator data</b>	<b>10</b>
3.1 Impact of $\theta_{13}$ on the atmospheric and LBL $\nu_\mu$ disappearance data	11
3.2 $\nu_\mu \rightarrow \nu_e$ appearance results in MINOS	13
<b>4. Global results and conclusions</b>	<b>14</b>

---

## 1. Introduction

It is now an established fact that neutrinos are massive and leptonic flavors are not symmetries of Nature [1, 2]. In the last decade this picture has become fully proved thanks to the upcoming of a set of precise experiments. In particular, the results obtained with solar and atmospheric neutrinos have been confirmed in experiments using terrestrial beams: neutrinos produced in nuclear reactors and accelerators facilities have been detected at distances of the order of hundreds of kilometers [3].

The minimum joint description of all the neutrino data requires mixing among all the three known neutrinos ( $\nu_e, \nu_\mu, \nu_\tau$ ), which can be expressed as quantum superpositions of three massive states  $\nu_i$  ( $i = 1, 2, 3$ ) with masses  $m_i$ . This implies the presence of a leptonic mixing matrix in the weak charged current interactions [4, 5] which can be parametrized as:

$$U = \begin{pmatrix} c_{12}c_{13} & s_{12}c_{13} & s_{13}e^{-i\delta_{\text{CP}}} \\ -s_{12}c_{23} - c_{12}s_{13}s_{23}e^{i\delta_{\text{CP}}} & c_{12}c_{23} - s_{12}s_{13}s_{23}e^{i\delta_{\text{CP}}} & c_{13}s_{23} \\ s_{12}s_{23} - c_{12}s_{13}c_{23}e^{i\delta_{\text{CP}}} & -c_{12}s_{23} - s_{12}s_{13}c_{23}e^{i\delta_{\text{CP}}} & c_{13}c_{23} \end{pmatrix}, \quad (1.1)$$

where  $c_{ij} \equiv \cos \theta_{ij}$  and  $s_{ij} \equiv \sin \theta_{ij}$ . In addition to the Dirac-type phase  $\delta_{\text{CP}}$ , analogous to that of the quark sector, there are two physical phases associated to the Majorana character of neutrinos, which however are not relevant for neutrino oscillations [6, 7] and are therefore omitted on the present work. Given the observed hierarchy between the solar and atmospheric mass-squared splittings there are two possible non-equivalent orderings for the mass eigenvalues, which are conventionally chosen as

$$\Delta m_{21}^2 \ll (\Delta m_{32}^2 \simeq \Delta m_{31}^2) \text{ with } (\Delta m_{31}^2 > 0); \quad (1.2)$$

$$\Delta m_{21}^2 \ll |\Delta m_{31}^2 \simeq \Delta m_{32}^2| \text{ with } (\Delta m_{31}^2 < 0). \quad (1.3)$$

As it is customary we refer to the first option, Eq. (1.2), as the *normal* scheme, and to the second one, Eq. (1.3), as the *inverted* scheme; in this form they correspond to the two possible choices of the sign of  $\Delta m_{31}^2$ . In this convention the angles  $\theta_{ij}$  can be taken without loss of generality to lie in the first quadrant,  $\theta_{ij} \in [0, \pi/2]$ , and the CP phase  $\delta_{\text{CP}} \in [0, 2\pi]$ .

Within this context,  $\Delta m_{21}^2$ ,  $|\Delta m_{31}^2|$ ,  $\theta_{12}$ , and  $\theta_{23}$  are relatively well determined [3, 8–10], while only an upper bound is derived for the mixing angle  $\theta_{13}$  and barely nothing is known on the CP phase  $\delta_{\text{CP}}$  and on the sign of  $\Delta m_{31}^2$ . Apart from the importance from a theoretical point of view, establishing whether  $\theta_{13}$  is zero or not is an essential step in the development of the search strategies for the upcoming experiments. Once we know that the two mixing angles  $\theta_{12}$  and  $\theta_{23}$  are relatively large, the possibility of experimentally accessing leptonic CP violation crucially depends on the value of the angle  $\theta_{13}$ . Also a non-zero  $\theta_{13}$  is a fundamental ingredient for a feasible determination of the neutrino mass ordering. For this reason, it is a main objective of upcoming reactor and accelerator experiments to directly measure this parameter. In this respect, Refs. [11, 12] pointed out that two independent hints in favor of a non-zero value of  $\theta_{13}$  emerge from the combination of solar and long-baseline (LBL) reactor data as well as from the combination of atmospheric, short-baseline reactor and LBL accelerator data. Since these signals are the results of synergies between different data samples, it is particularly important to verify their stability with respect to new experimental data as well as to variations on the assumptions in the analysis.

In this work we present the results of an up-to-date global analysis of solar, atmospheric, reactor and LBL accelerator neutrino data in the context of three-neutrino oscillations. In Sec. 2 we focus on the solar sector and we assess the stability of the oscillation parameters with respect to the inclusion of the new experimental results and theoretical advances which have become public during the last year. In this context, we find that many of these changes indeed lower the statistical significance of a non-zero value of  $\theta_{13}$ . In Sec. 3 we do the same in the atmospheric sector, with particular emphasis on the recent  $\nu_e$  appearance results from MINOS and the recent Super-Kamiokande results from the combined phases I, II and III. In Sec. 4 we combine all the data together and we determine the presently allowed ranges of mass and mixing, thus updating our previous results.

## 2. Leading $\Delta m_{21}^2$ oscillations: solar and KamLAND data

In the analysis of solar neutrino experiments we include the total rates from the radiochemical experiments Chlorine [13], Gallex/GNO [14]<sup>1</sup> and SAGE [16]. For real-time experiments we include the 44 data points of the electron scattering (ES) Super-Kamiokande phase I (SK-I) energy-zenith spectrum [17] and the data from the three phases of SNO [18–20], including the results on the low energy threshold analysis of the combined SNO phase I and phase II [21] (which we label SNO-LETA). We also include the main set of the 192 days of Borexino data [22] (which we label Borexino-LE) as well as their high-energy spectrum from 246 live days [23] (Borexino-HE). We consider the following variations on the analysis:

---

<sup>1</sup>Note that the value  $R_{\text{Gallex}} = 73.4^{+6.1}_{-6.0}$  (stat)  $^{+3.7}_{-4.1}$  (syst) SNU presented in [14] fully coincide with the preliminary result quoted in [15], and has been commonly used in the literature since 2008.

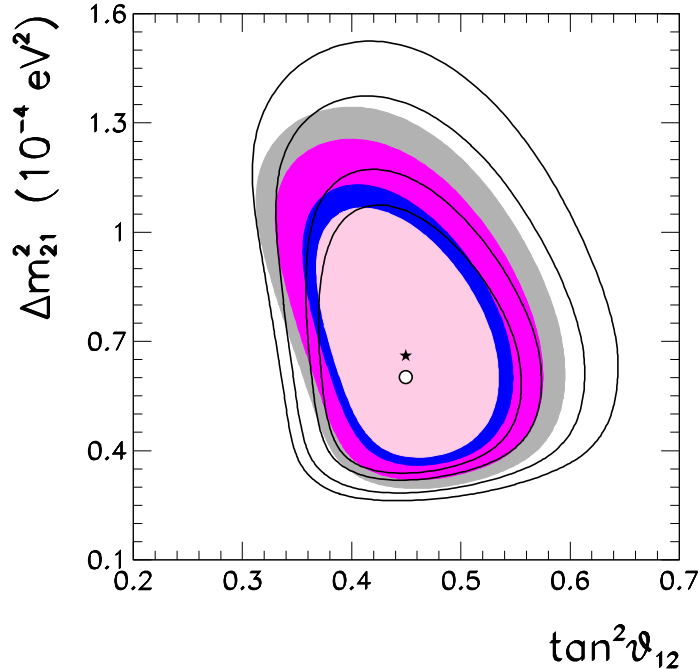


**Figure 1:** Allowed parameter regions (at 90%, 95%, 99% and 99.73% CL for 2 d.o.f.) from the combined analysis of solar data for  $\theta_{13} = 0$ . The best-fit point is marked with a star. For comparison we also show as empty regions (the best-fit is marked by a circle) the results prior to the inclusion of the latest Ga capture rate of SAGE [16], the energy spectrum of Borexino [22, 23] and the low energy threshold analysis of the combined SNO phase I and phase II [21]. In both analysis we use as inputs the GS98 solar model fluxes and the Gallium capture cross-section of Bahcall [24].

- **Updated capture rate in gallium.** In Ref. [16] the Russian-American experiment SAGE has presented the results of the combined analysis of 168 extractions (until December 2007). The capture rate of solar neutrinos above the 233 keV threshold is

$$R_{\text{SAGE}}^{09} = 65.4_{-3.0}^{+3.1} (\text{stat})_{-2.8}^{+2.6} (\text{syst}) \text{ SNU}. \quad (2.1)$$

which is slightly lower (but fully consistent) than the previous result quoted in Ref. [15],  $66.2_{-3.2}^{+3.3} (\text{stat})_{-3.2}^{+3.5} (\text{syst}) \text{ SNU}$ , and presents a considerable improvement of the systematic uncertainties.

- **Possible modification of the capture cross-section in gallium.** Ref. [16] also presents the results of a new calibration of the SAGE detector with a reactor-produced  $^{37}\text{Ar}$  neutrino source. The ratio of observed to expected event rate in this experiment, once combined with the measured rates in the three prior  $^{51}\text{Cr}$  neutrino-source experiments with Gallium, is  $0.87 \pm 0.05$ . As a possible explanation for this low result, in Ref. [16] it is proposed that the cross-section for neutrino capture by the two lowest-lying excited states in  $^{71}\text{Ge}$  may have been overestimated in Ref. [24]. As an alternative, the authors consider a modified capture cross-section where the contribution from these two excited states is set to zero.

- **Inclusion of the Borexino spectral data.** Following the procedure described in Ref. [25] (see Appendix A of that work for details) we have included in the analysis the 160 data points of the Borexino energy spectrum in the 365–2000 keV energy range [22] as well as the 7 points of the high-energy spectrum from the 246 live days of Borexino [23]. In our approach the overall normalizations of the  $^{11}\text{C}$ ,  $^{14}\text{C}$ ,  $^{210}\text{Bi}$  and  $^{85}\text{Kr}$  backgrounds are introduced as free parameters and are fitted to the data.
- **Low energy threshold analysis of the combined SNO phase I and phase II data.** In Ref. [21] the SNO Collaboration reported the results from a joint analysis of their Phase I and Phase II data with an effective electron kinetic energy threshold of  $T_{\text{eff}} = 3.5$  MeV. Besides the inclusion of the lower energy data the analysis present improvements in the calibration and analysis techniques to reduce the threshold and increase the precision of the results.

From the point of view of any reanalysis of their data, there is an important difference with respect to the previous higher threshold results. In Refs. [18,19] the results were quoted in the form of binned (in energy and time) event rates. In particular, 34 data points of the day-night spectrum were given for SNO-I, and the separate day and night rates for neutral current (NC) and ES events as well as the day-night energy-spectrum for charge current (CC) events were given for SNO-II. Instead, in Ref. [21] the collaboration presents its reanalysis as a total  $^8\text{B}$  neutrino flux plus an effective description (under the assumption of unitarity for active neutrinos) of the  $\nu_e$  survival probability, whose dependence on  $E_\nu$  is parametrized as a quadratic function for  $P_{ee}^{\text{day}}$  and a linear function for the day/night asymmetry. In other words, the SNO-LETA results are given as best-fit, uncertainties and correlations of six effective parameters: the  $^8\text{B}$  flux, three polynomial coefficients of  $E_\nu$  for the  $P_{ee}^{\text{day}}$  and two for the day-night asymmetry. When using these data to perform a fit to neutrino oscillations, for each value of the oscillation parameters one must first obtain the polynomial coefficients that best represent the corresponding Mikheev, Smirnov and Wolfenstein (MSW) [26, 27] oscillation probability. This has to be done taking into account the sensitivity of the SNO detector, and the relevant information is provided in the Appendix A of Ref. [21]. We have followed the procedure outlined there and we have verified that we can perfectly reproduce their oscillation results in Fig. 37.<sup>2</sup>

- **Uncertainties on the Solar Model.** Recent detailed determination of the abundances of the heavy elements on the solar surface [28,29] lead to lower values than previous studies [30]. Any solar model which incorporates such lower metallicities fails at explaining the helioseismological observations [31]. Changes in the Sun modeling, in particular of the less known convective zone, are not able to account for this discrepancy [32,33]. So far there has not been a successful solution of this puzzle, so

---

<sup>2</sup>However we notice that this procedure does not allow the inclusion of the SNO low energy threshold data in analysis in terms of more exotic scenarios in which either unitarity in the active neutrino sector does not hold (like for scenarios with sterile neutrinos) or the energy dependence of the oscillation probability cannot be well represented by a simple quadratic function.

that at present there is no fully consistent Standard Solar Model (SSM). This lead to the construction of two different sets of SSM's, one (labeled “GS”) based on the older solar abundances [30] leading to high metallicity, and one (labeled “AGS”) assuming lower metallicity [34]. We use the most recent recalculation of the fluxes in these two sets from Ref. [35], and following their notation we refer to them as GS98 and AGSS09.

Let us first consider the case  $\theta_{13} = 0$ . In Fig. 1 we show the present determination of the leading parameters  $\Delta m_{21}^2$  and  $\theta_{12}$  from the updated oscillation analysis of the solar neutrino data described above in the context of the GS98 solar model. For comparison we also show the results obtained prior to the inclusion of the latest Ga capture rate of SAGE [16], the energy spectrum of Borexino [22, 23] and the SNO-LETA results [21] for the same solar model. As seen in this figure, the inclusion of these results lead to an improvement on the determination of both  $\theta_{12}$  and  $\Delta m_{21}^2$  and for this last one the best-fit value slightly increases. The effect of the different variations in the analysis is displayed in Fig. 2, where we show the 99% CL region in the  $(\Delta m_{21}^2, \tan^2 \theta_{12})$  plane from the present analysis and the corresponding one when some of the input data or assumption are modified. The figure shows that the most quantitatively relevant new information arises from the inclusion of the SNO-LETA results. The inclusion of Borexino tends to shift the region towards slightly lower values of  $\theta_{12}$  angle. Conversely, if the analysis is done in the context of the AGSS09 model the region is shifted towards slightly larger  $\theta_{12}$ .

## 2.1 Impact of $\theta_{13}$ on the solar analysis

The survival probability of solar neutrinos in the framework of three neutrino oscillations can be written as:

$$P_{ee}^{3\nu} = \sin^4 \theta_{13} + \cos^4 \theta_{13} P_{ee}^{2\nu}(\Delta m_{21}^2, \theta_{12}), \quad (2.2)$$

where we have used the fact that  $L_{31}^{\text{osc}} = 4\pi E/\Delta m_{31}^2$  is much shorter than the distance between the Sun and the Earth, so that the oscillations related to  $L_{31}^{\text{osc}}$  are averaged. In presence of matter effects  $P_{ee}^{2\nu}(\Delta m_{21}^2, \theta_{12})$  should be calculated taking into account the evolution in an effective matter density  $n_e^{\text{eff}} = n_e \cos^2 \theta_{13}$ . For  $10^{-5} \lesssim \Delta m^2/\text{eV}^2 \lesssim 10^{-4}$ ,  $P_{ee}^{2\nu}(\Delta m_{21}^2, \theta_{12})$  presents the following asymptotic behaviors [36]:

$$P_{ee}^{2\nu}(\Delta m_{21}^2, \theta_{12}) \simeq 1 - \frac{1}{2} \sin^2(2\theta_{12}) \quad \text{for } E_\nu \lesssim \text{few} \times 100 \text{ KeV} \quad (2.3)$$

$$P_{ee}^{2\nu}(\Delta m_{21}^2, \theta_{12}) \simeq \sin^2(\theta_{12}) \quad \text{for } E_\nu \gtrsim \text{few} \times 1 \text{ MeV} \quad (2.4)$$

The impact of the inclusion of a non-zero value of  $\theta_{13}$  in the solar analysis is shown in Fig. 3 and in the upper-left panel of Fig. 4. From this last plot we see that solar neutrino data by themselves favor  $\theta_{13} = 0$ , although their sensitivity is very weak for  $\sin^2 \theta_{13} \lesssim 0.03$ . This behavior can be understood from Fig. 3, where we show the allowed regions (at 95% CL) in the  $(\Delta m_{21}^2, \tan^2 \theta_{12})$  plane as obtained from the analysis of low-energy (radiochemical and Borexino-LE) and high-energy (SK, SNO and Borexino-HE) solar experiments, for different values of  $\theta_{13}$ . As described in Eq. (2.2), for fixed values of  $\Delta m_{21}^2$  and  $\theta_{12}$ , the inclusion of a small value of  $\theta_{13}$  results into a decrease on the predicted

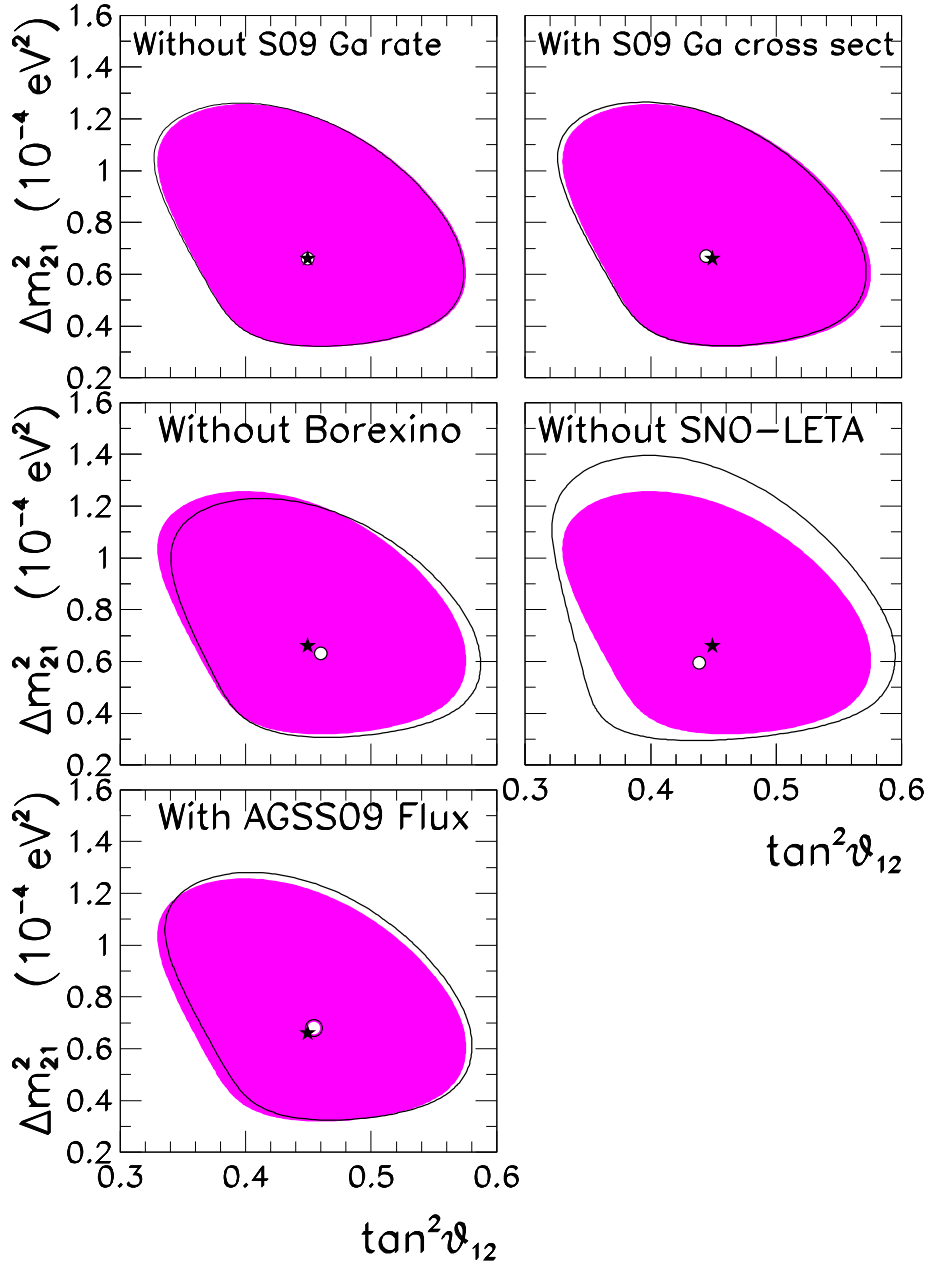


**Figure 2:** Effects of the different assumed inputs on the 99% CL parameter region from the combined analysis of solar data for  $\theta_{13} = 0$ . The full region corresponds to the results show in Fig. 1. The solid line corresponds to the modification due to the change on one of the inputs as labeled in each panel.

rates at a given solar neutrino experiment. This decrease can be compensated by a shift of  $\Delta m_{21}^2$  and  $\theta_{12}$  which lead to an increase of  $P_{ee}^{2\nu}$ . However the sign of the shift strongly depends on the characteristic energy of the detected neutrinos. For experiments detecting neutrinos with energies low enough for matter effects to be irrelevant (such as Chlorine and Gallium experiments)  $P_{ee}^{2\nu}$  is given by Eq. (2.3) and increases as  $\theta_{12}$  decreases. Conversely,

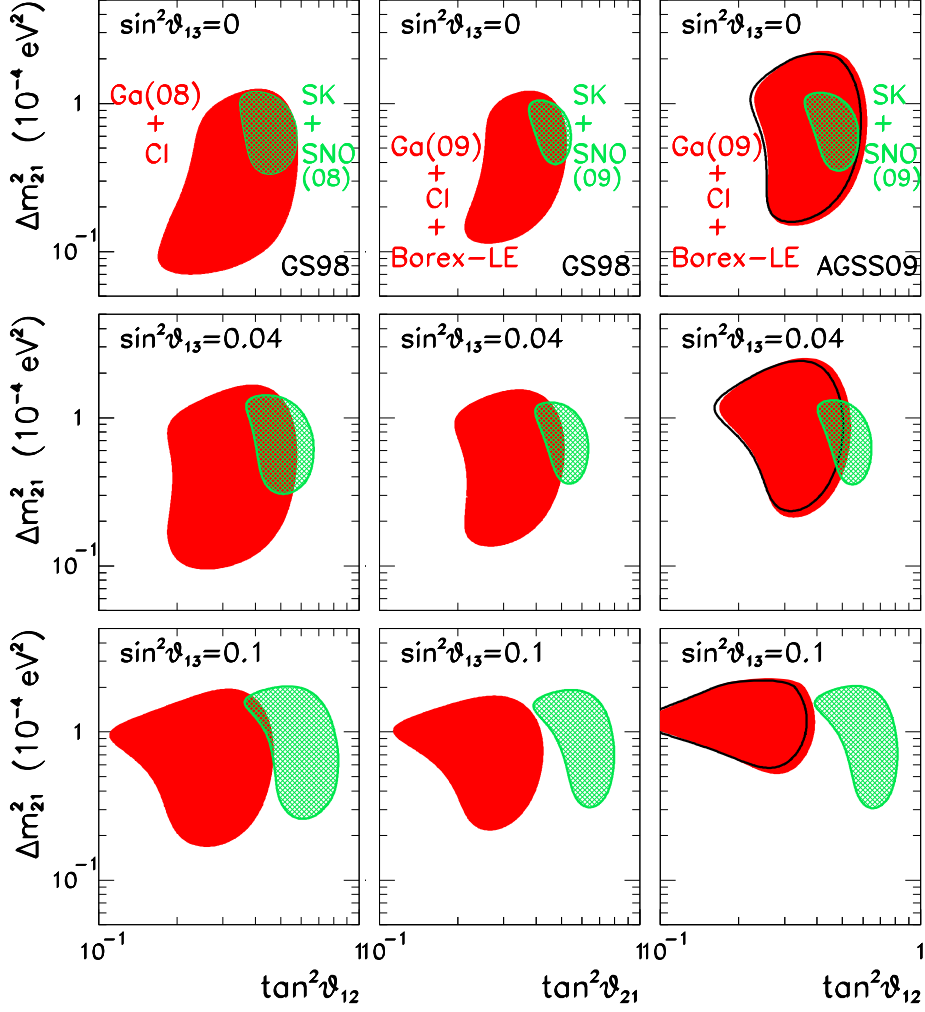


**Figure 3:** Dependence on  $\theta_{13}$  of the allowed  $(\Delta m_{21}^2, \tan^2 \theta_{12})$  regions (at 95% CL for 2 d.o.f.) from the partial analysis of the “low energy” and “high energy” solar neutrino data. The left column corresponds to the analysis prior to the inclusion of the latest Ga capture rate of SAGE [16], the energy spectrum of Borexino [22, 23] and the low energy threshold analysis of the combined SNO phase I and phase II [21]. In the central and right columns the results of those experiments are included. The central column corresponds to GS98 solar model fluxes and Gallium capture cross-section of Bahcall [24]. In the right panels the AGSS09 solar model fluxes are used. The full (void) regions are obtained with Gallium capture cross-section of Bahcall [24] (modified cross-section in Ref. [16]).

for experiments detecting neutrinos mostly in the regime of adiabatic matter oscillations (such as SK and SNO)  $P_{ee}^{2\nu}$  is given by Eq. (2.4) and increases as  $\theta_{12}$  increases. Consequently the combined fit worsens with  $\theta_{13}$ .

Fig. 3 also illustrates how the inclusion of the new data strengthens this tension. The quantitative improvement on the corresponding bound on  $\theta_{13}$  is displayed in the upper-left panel of Fig. 4. We have also studied the dependence of this result on the assumed solar model and on the possible modification of the neutrino capture in gallium. We find that



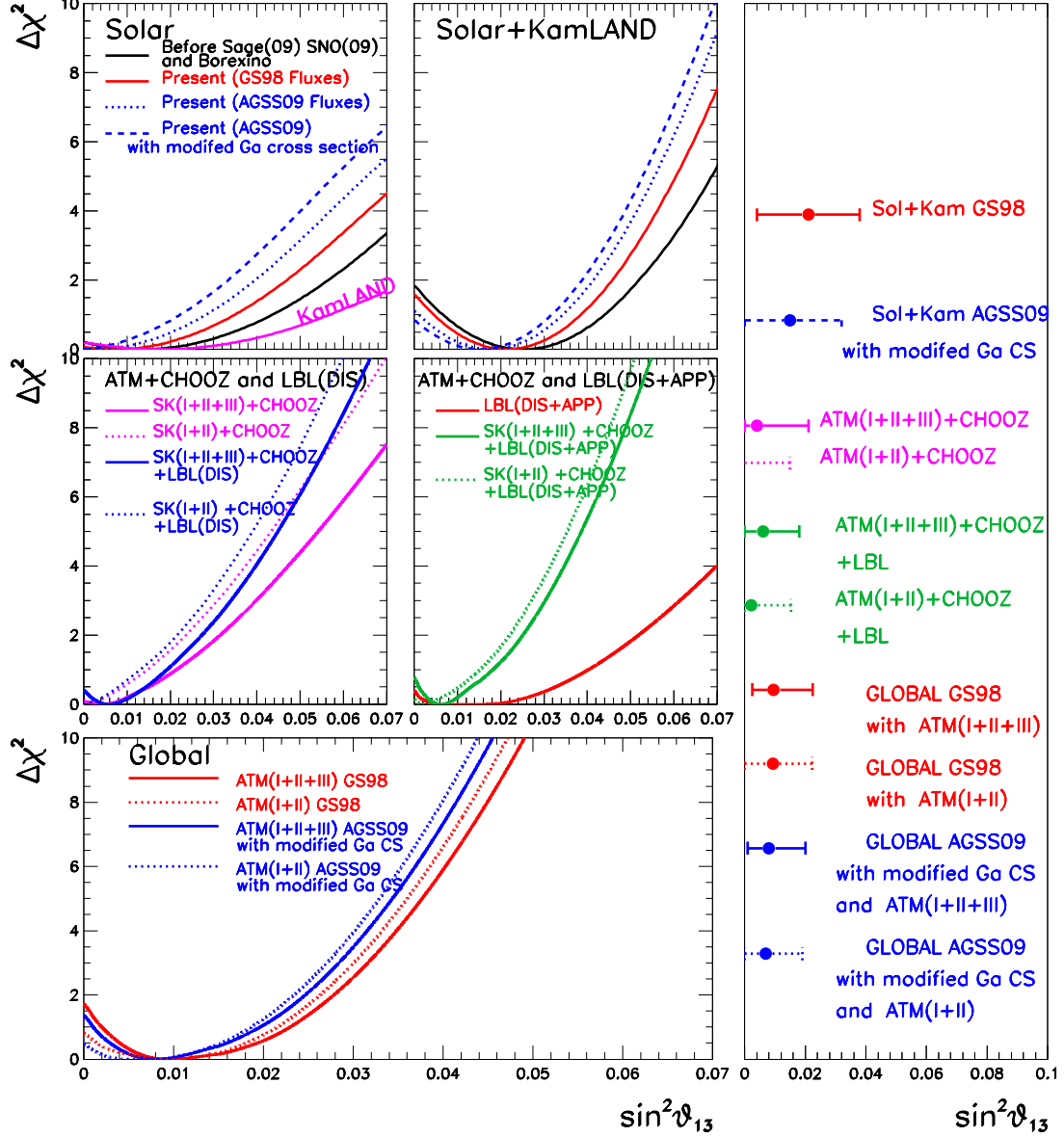


**Figure 4:** Dependence of  $\Delta\chi^2$  on  $\sin^2\theta_{13}$  for the different analysis as labeled in the figure and the corresponding  $1\sigma$  ranges.

the AGSS09 fluxes lead to a stronger bound on  $\theta_{13}$  and the same happens with the modified gallium cross-section. This second effect can be easily understood as follows: because of the lower cross-section, a slightly larger survival probability is required to fit the same data. This shifts the  $(\Delta m_{21}^2, \tan^2\theta_{12})$  allowed region obtained from the analysis of the radiochemical solar experiments towards slightly lower values of  $\theta_{12}$  (as explicitly shown in the last column of Fig. 3). As a consequence it increases the tension with the SNO+SK favored mixing angle for non-zero  $\theta_{13}$ .

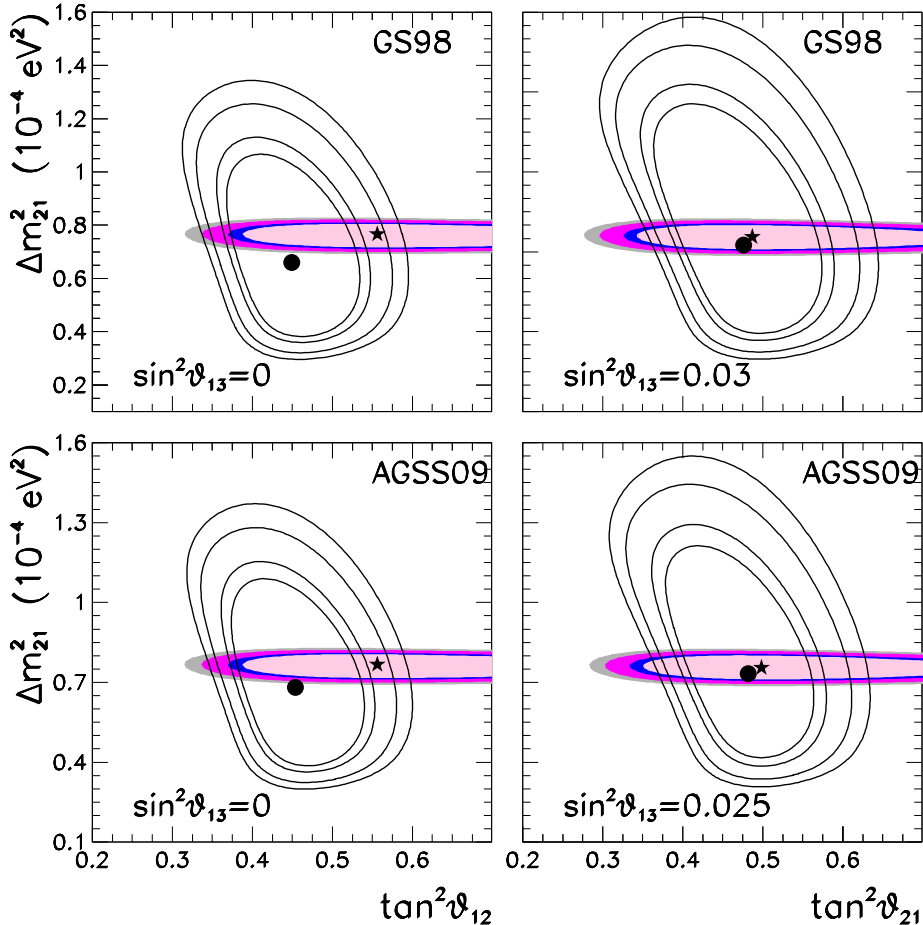


**Figure 5:** Allowed parameter regions (at 90%, 95%, 99% and 99.73% CL for 2 d.o.f.) from analysis of KamLAND (full regions with best-fit marked by a star) and solar (void regions with best-fit marked by a dot) data for two values of  $\theta_{13}$  as labeled in the figure and for the two solar models.

## 2.2 Combination with KamLAND and the hint of $\theta_{13} \neq 0$

We show in the left panels of Fig. 5 the present determination of the leading parameters  $\Delta m_{21}^2$  and  $\theta_{12}$  (for  $\theta_{13} = 0$ ) from the analysis of KamLAND spectral data [37] compared to those from the updated solar analysis for the two solar models considered. While the results show perfect agreement in  $\Delta m_{21}^2$ , there appears to be a mismatch in the favored value of  $\theta_{12}$  as determined from KamLAND compared to the one from solar neutrinos, this last one being mostly sensitive to the precise value of CC/NC event (*i.e.*, to  $\langle P_{ee} \rangle \propto \sin^2 \theta_{12}$ ) as determined by SK and SNO.

As it was pointed out in Ref. [11] and widely discussed in the literature [8–10,38], this mismatch can be lifted by a non-zero value of  $\theta_{13}$ . This happens because, as discussed above, the CC/NC event rate can be fitted with a higher value of  $\theta_{12}$  provided that a non-zero  $\theta_{13}$  is included. Conversely for KamLAND Eq. (2.2) also holds with

$$P_{ee}^{2\nu, \text{kam}} = 1 - \frac{1}{2} \sin^2(2\theta_{12}) \sin^2 \frac{\Delta m_{21}^2 L}{2E}. \quad (2.5)$$

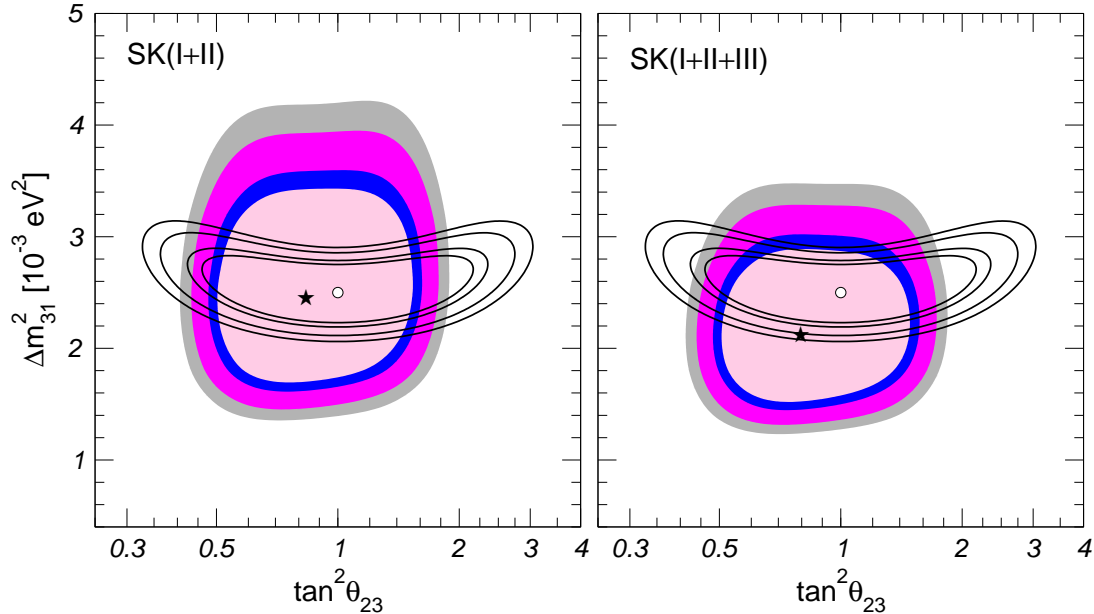


**Figure 6:** Allowed parameter regions (at 90%, 95%, 99% and 99.73% CL for 2 d.o.f.) from the analysis of atmospheric data (full regions, best-fit marked with a star) and LBL data (void regions, best-fit marked by a circle) for  $\theta_{13} = 0$  and  $\Delta m_{21}^2 = 7.6 \times 10^{-5} \text{ eV}^2$ .

So for  $\theta_{13} > 0$  the KamLAND spectrum can be well fitted with a smaller value of  $\theta_{12}$ , and consequently the best-fit values for solar and KamLAND analysis agree better for  $\theta_{13} \neq 0$ . This behavior is clearly visible in the right panels of Fig. 5 and in the upper-central panel of Fig. 4. As mentioned before, the best-fit value of  $\theta_{12}$  for solar neutrino fit within the AGSS09 model is slightly larger than for the GS98 model, and therefore the required value of  $\theta_{13}$  to achieve agreement with KamLAND is smaller for the AGSS09 model.

However, one must notice that the better agreement between the solar and KamLAND analysis for  $\theta_{13} \neq 0$  has to be contrasted with the worsening of the global description of the solar neutrino data previously described. As a consequence of this tension we find that the inclusion of the new data and of the modified gallium capture cross-section also tend to lower the best-fit value of  $\theta_{13}$  as well as its corresponding statistical significance (see upper-central panel of Fig. 4). Altogether we find that the  $1\sigma$  range for  $\theta_{13}$  as determined from the global analysis of solar and KamLAND data changes from the old value  $\sin^2 \theta_{13} = 0.025 \pm 0.018$  (before the inclusion of SNO-LETA, SAGE-09 and Borexino data) to:

$$\sin^2 \theta_{13} = \begin{cases} 0.021 \pm 0.017 & \text{for GS98,} \\ 0.017 \pm 0.017 & \text{for AGSS09,} \\ 0.015 \pm 0.017 & \text{for AGSS09 with modified Ga cross-section.} \end{cases} \quad (2.6)$$

### 3. Leading $\Delta m_{31}^2$ oscillations: atmospheric, CHOOZ and accelerator data

In this section we present two different analyses of the atmospheric data. The first one is very similar to the one detailed in Ref. [3], and includes the results from the first run

of Super-Kamiokande, which accumulated data from May 1996 to July 2001 (1489 day exposure) and is usually referred as SK-I [39], as well as the data obtained with the partial coverage after the 2001 accident (804 day exposure), the so-called SK-II period [40]. We will refer to this analysis as SK(I+II). The second one is based on the new analysis recently presented by the Super-Kamiokande collaboration including also the data taken from December 2005 to June 2007, usually referred as SK-III [41]. Apart from the inclusion of these new event rates, in this data release the selection criteria and the corresponding estimate of uncertainties for the SK-I and SK-II periods have been changed with respect to the previous SK(I+II) analysis. We have therefore performed a reanalysis of the new combined samples from phases I, II and III as presented in [41]. We refer to the results of this analysis as SK(I+II+III). It is important to point out that already since SK-II the Super-Kamiokande collaboration has been presenting its experimental results in terms of a large number of data samples. The rates for some of those samples cannot be theoretically predicted (and therefore include in a statistical analysis) without a detailed simulation of the detector which can only be made by the experimental collaboration itself. Thus our results represent the most up-to-date analysis of the atmospheric neutrino data which can be performed outside the collaboration. For details on our simulation of the data samples and the statistical analysis see the Appendix of Ref. [3].

For what concerns LBL accelerator experiments, we combine the results on  $\nu_\mu$  disappearance from K2K [42] with those obtained by MINOS at a baseline of 735 km after a two-year exposure to the Fermilab NuMI beam, corresponding to a total of  $3.36 \times 10^{20}$  protons on target [43]. We also include the recent results on  $\nu_\mu \rightarrow \nu_e$  transitions based on an exposure of  $7 \times 10^{20}$  protons on target [44,45].

In order to test the description of the present data in the absence of  $\theta_{13}$ -induced effects we show in Fig. 6 the present determination of the leading parameters  $\Delta m_{31}^2$  and  $\theta_{23}$  for  $\theta_{13} = 0$  and  $\Delta m_{21}^2 = 7.6 \times 10^{-5} \text{ eV}^2$  from the two atmospheric neutrino analyses and the LBL accelerator results. For concreteness we plot only normal ordering; the case of inverted ordering gives practically identical results as long as  $\theta_{13} = 0$ . This figure illustrates how the bounds on the oscillation parameters  $\theta_{23}$  and  $\Delta m_{31}^2$  emerges from a complementarity of atmospheric and accelerator neutrino data:  $|\Delta m_{31}^2|$  is determined by the spectral data from MINOS, whereas the mixing angle  $\theta_{23}$  is still largely dominated by atmospheric data from Super-Kamiokande with a best-fit point close to maximal mixing. It is important to note that there is a very good agreement in the location of the best-fit points from SK(I+II) and MINOS. This is not the case for SK(I+II+III) for which the best-fit point in  $|\Delta m_{31}^2|$  is now lower than the one obtained from LBL. In what follows we will discuss the impact of this tension on the allowed range of  $\theta_{13}$ .

### 3.1 Impact of $\theta_{13}$ on the atmospheric and LBL $\nu_\mu$ disappearance data

It is well known that a very important contribution to our knowledge of  $\theta_{13}$  arises from the negative results on  $\bar{\nu}_e$  disappearance at short baselines at the CHOOZ reactor experiment [46]. Given the values of  $\Delta m_{21}^2$  obtained from solar and KamLAND experiments, the disappearance of  $\bar{\nu}_e$  at the CHOOZ distances arises from oscillations due to  $|\Delta m_{31}^2|$  whose amplitude is proportional to  $\sin^2(2\theta_{13})$ . Consequently, when combined with the bounds on

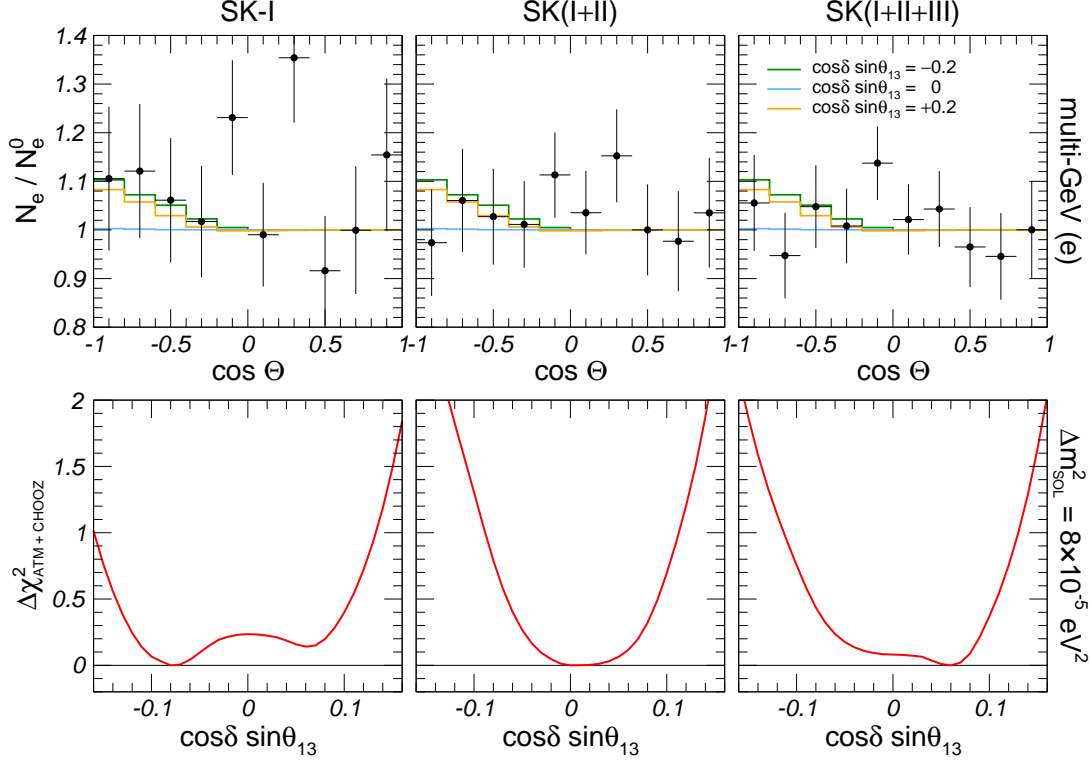


**Figure 7:** Zenith distribution for multi-GeV  $e$ -like events (upper panels), and  $\Delta\chi^2$  dependence on  $\cos\delta_{\text{CP}}\sin\theta_{13}$  marginalized over all undisplayed parameters (lower panels). The fits include the CHOOZ data as well as the full atmospheric data samples for SK-I (left panels), SK-I with modified multi-GeV  $e$ -like data (central-left panels), SK(I+II) (central-right panels) and SK(I+II+III) (right panels).

$|\Delta m_{31}^2|$  from atmospheric and  $\nu_\mu$  disappearance at LBL experiments the CHOOZ result implies an upper bound on  $\theta_{13}$ .

In Ref. [11] a hint for a non-zero value of  $\theta_{13}$  was obtained at  $0.9\sigma$  from the analysis of atmospheric data from SK-I,  $\nu_\mu$  disappearance at long-baseline experiments and CHOOZ. The authors traced its origin to subleading effects driven by  $\Delta m_{21}^2$ . This result was extensively studied in Ref. [10], where it was pointed out that the appearance of the hint is triggered by an excess of multi-GeV  $e$ -like data in the first two angular bins of SK-I data, which lead to a better fit for this sample in the case of a non-zero value of  $\theta_{13}$ . This conclusion is summarized in Fig. 7: as clearly visible in the leftmost panel, there is a small but definite preference for a non-zero value of  $\theta_{13}$  in SK-I. Once the SK-II data are included in the analysis the event rates of those bins are considerably reduced, and as a consequence no hint of non-zero  $\theta_{13}$  is found in SK(I+II). As can be seen in the rightmost panels, in the new SK(I+II+III) data release there is again a small excess in the first angular bin of multi-GeV  $e$ -like data, and consequently a weak preference for non-zero  $\theta_{13}$  reappears. Such “hint”, however, is considerably weaker than in the SK-I case and completely negligible from the statistical point of view.

In order to better understand the impact of the various data samples, in the second

row of Fig. 4 we plot the bound on  $\theta_{13}$  as implied by different combinations of atmospheric and LBL experiments. In all panels the results are marginalized with respect to the undisplayed parameters, and in particular to the sign of  $\Delta m_{31}^2$ . As can be seen, for both SK(I+II) and SK(I+II+III) the combined analysis of atmospheric and CHOOZ show no relevant preference for nonzero  $\theta_{13}$ , and the data results exclusively into a bound on  $\theta_{13}$ . Such bound is weaker for SK(I+II+III) as a result of the lower values of  $|\Delta m_{31}^2|$  preferred by the atmospheric analysis, and gets slightly strengthened by the inclusion of LBL  $\nu_\mu$  disappearance data. Since the  $\nu_\mu$  survival probability at MINOS and K2K is practically insensitive to such small values of  $\theta_{13}$ , this improvement arises as an indirect effect driven by the better determination of  $|\Delta m_{31}^2|$ . On the other hand, it should be noted that when combining the new SK(I+II+III) with LBL  $\nu_\mu$  disappearance data a small preference for a non-zero value of  $\theta_{13}$  arises. This effect is a consequence of the mismatch between the best-fit  $|\Delta m_{31}^2|$  in atmospheric and MINOS data shown in Fig. 6. Within our atmospheric neutrino analysis this is only a  $\Delta\chi^2 = 0.5$  effect. However, the analysis of the atmospheric data presented in Ref. [41] by Super-Kamiokande seems to exhibit a non-negligible dependence of the preferred  $\Delta m_{31}^2$  range on  $\theta_{13}$  (see, *e.g.*, the leftmost panels of Figs. 7 and 8 in [41]). It would therefore be very interesting if the Super-Kamiokande and MINOS collaborations could perform a combined analysis of their samples in order to fully establish the statistical significance of this effect.

### 3.2 $\nu_\mu \rightarrow \nu_e$ appearance results in MINOS

In Ref. [47] the MINOS collaboration reported their first results on the search for  $\nu_\mu \rightarrow \nu_e$  transitions based on an exposure of  $3.14 \times 10^{20}$  protons-on-target in the Fermilab NuMI beam. They observed 35 events in the Far Detector with a background of  $27 \pm 5$  (stat)  $\pm 2$  (syst) events predicted by their measurements in the Near Detector. This result corresponded to a  $1.5\sigma$  excess which could be explained by a non-zero value of  $\theta_{13}$ . Recently a new analysis with double statistics (exposure of  $7 \times 10^{20}$ ) has been presented [44,45]. The MINOS collaboration reported the observation of 54 events with an expected background of  $49.1 \pm 7.0$  (stat)  $\pm 2.7$  (syst), thus reducing the excess above background to  $0.7\sigma$ .

In the left panel of Fig. 8 we show the reconstructed energy distribution of the observed events together with the background expectations. We compare our simulation of the expected spectrum in the presence of  $\nu_\mu \rightarrow \nu_e$  oscillations with the one given by the MINOS collaboration. In the right panel of Fig. 8 we perform an oscillation analysis of the MINOS total event rate, and again we compare our limits on  $\theta_{13}$  for given  $\delta_{CP}$  to those obtained by the MINOS collaboration. In both cases we find perfect agreement.

In the central panel of Fig. 4 we show the information on  $\theta_{13}$  from the analysis of the LBL data from both  $\nu_e$  appearance and  $\nu_\mu$  disappearance and its impact when combined with the atmospheric and CHOOZ data. As seen in this figure, the inclusion of MINOS appearance data in combination with either atmospheric neutrino samples leads to a stronger upper bound on  $\theta_{13}$ . Due to the  $0.7\sigma$  excess it also increases slightly the significance for  $\theta_{13} \neq 0$ . As expected, this increase is larger when combined with SK(I+II+III), since in this case the MINOS  $\nu_e$  appearance excess adds to the  $\Delta m_{31}^2$  mismatch effect between SK(I+II+III) and MINOS  $\nu_\mu$  disappearance discussed above. Altogether we find that the

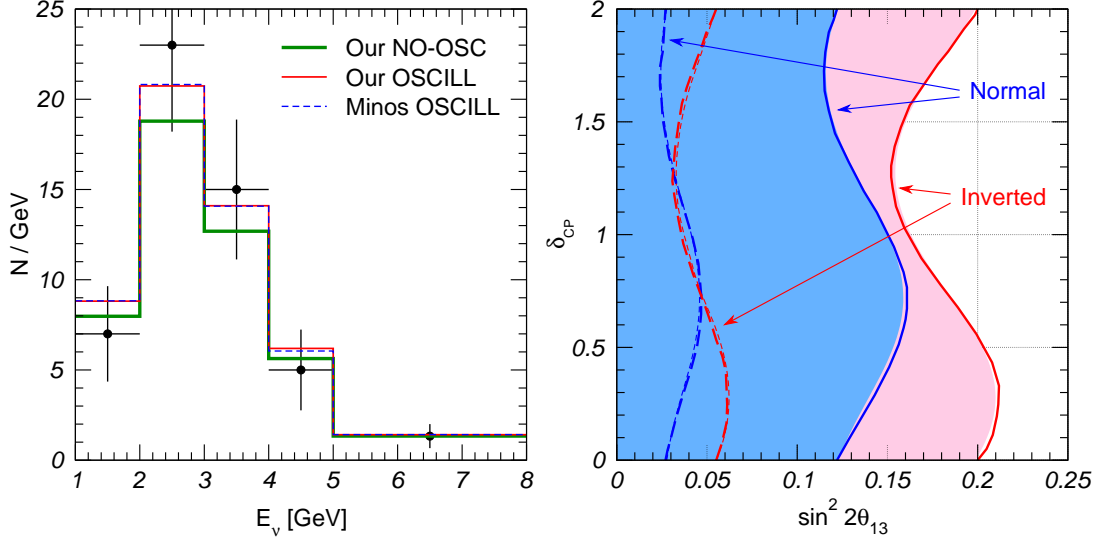


**Figure 8:** Left: reconstructed energy distribution of the  $\nu_e$  charged current events in the MINOS far detector. We show the background prediction (thick solid green line) as well as our (red solid) and MINOS (blue dashed) predictions for the expected spectrum in the presence of  $\nu_\mu \rightarrow \nu_e$  oscillations with  $\sin^2 2\theta_{13} = 0.115$  and  $\delta_{\text{CP}} = 0$ . Right: best-fit and upper bound on  $\theta_{13}$  as a function of  $\delta_{\text{CP}}$  for the MINOS  $\nu_e$  appearance data. The dashed (dotted) lines represent the best-fit as obtained from our (MINOS) analysis for normal and inverted ordering. The solid regions are our 90% bounds for normal (darker blue) and inverted (lighter red) ordering; the solid lines show the corresponding limits from MINOS, taken from Ref. [44]. In both panels the remaining parameters are fixed to  $\tan^2 \theta_{12} = 0.45$ , maximal  $\theta_{23}$ ,  $\Delta m_{21}^2 = 7.6 \times 10^{-5} \text{ eV}^2$  and  $|\Delta m_{32}^2| = 2.43 \times 10^{-3} \text{ eV}^2$ .

$1\sigma$  range for  $\theta_{13}$  as determined from the analysis of atmospheric, CHOOZ and LBL data reads:

$$\sin^2 \theta_{13} = 0.002_{-0.005}^{+0.013} \quad \text{CHOOZ + LBL(DIS+APP) + SK(I+II)}, \quad (3.1)$$

$$\sin^2 \theta_{13} = 0.006_{-0.007}^{+0.012} \quad \text{CHOOZ + LBL(DIS+APP) + SK(I+II+III)}, \quad (3.2)$$

where for the sake of illustration we have extrapolated the lower  $1\sigma$  bound to the unphysical region  $\sin^2 \theta_{13} < 0$ .

#### 4. Global results and conclusions

The results of the global combined analysis including the SK(I+II+III) atmospheric neutrino data and all dominant and subdominant oscillation effects are summarized in Fig. 9, where we show the different projections of the allowed six-dimensional parameter space. The full regions correspond to the analysis done in the framework of the GS98 solar model and with Ga capture cross-section in Ref. [24] while the void regions correspond to the analysis with AGSS09 solar fluxes and the modified Ga capture cross-section in Ref. [16]. The regions in each panel are obtained after marginalization of  $\chi_{\text{global}}^2$  with respect to the undisplayed parameters. In the lower panel we show the allowed regions in the  $(\sin^2 \theta_{13}, \delta_{\text{CP}})$  plane. As seen in the figure, at present the sensitivity to the CP phase is marginal but we

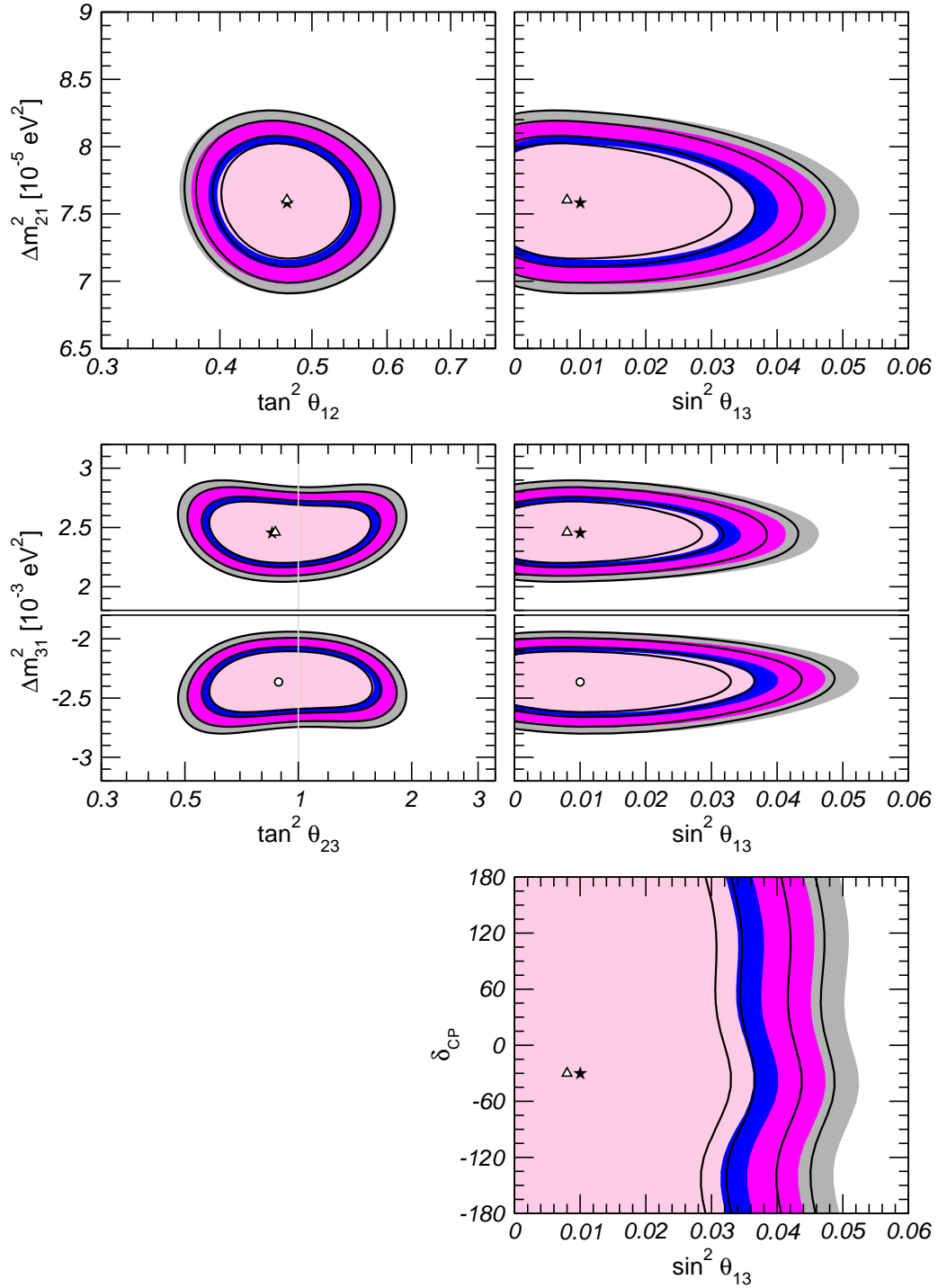


**Figure 9:** Global  $3\nu$  oscillation analysis. Each panels shows two-dimensional projection of the allowed five-dimensional region after marginalization with respect to the undisplayed parameters. The different contours correspond to the two-dimensional allowed regions at 90%, 95%, 99% and  $3\sigma$  CL. The full regions correspond to the analysis done in the framework of the GS98 solar model and with Ga capture cross-section in Ref. [24] while the void regions correspond to the analysis with AGSS09 solar fluxes and the modified Ga capture cross-section in Ref. [16].



find that the bound on  $\sin^2 \theta_{13}$  can vary by about  $\sim 30\%$  depending on the exact value of  $\delta_{\text{CP}}$ . This arises mainly from the interference of  $\theta_{13}$  and  $\Delta m_{21}^2$  effects in the atmospheric neutrino observables, as well as from the new MINOS  $\nu_e$  appearance data. The derived ranges for the six parameters at the  $1\sigma$  ( $3\sigma$ ) level are:

GS98 with Gallium cross-section from [24]	AGSS09 with modified Gallium cross-section [16]
$\Delta m_{21}^2 = 7.59 \pm 0.20 \left( \begin{smallmatrix} +0.61 \\ -0.69 \end{smallmatrix} \right) \times 10^{-5} \text{ eV}^2$	Same
$\Delta m_{31}^2 = \begin{cases} -2.36 \pm 0.11 (\pm 0.37) \times 10^{-3} \text{ eV}^2 \\ +2.46 \pm 0.12 (\pm 0.37) \times 10^{-3} \text{ eV}^2 \end{cases}$	Same
$\theta_{12} = 34.4 \pm 1.0 \left( \begin{smallmatrix} +3.2 \\ -2.9 \end{smallmatrix} \right)^\circ$	$34.5 \pm 1.0 \left( \begin{smallmatrix} +3.2 \\ -2.8 \end{smallmatrix} \right)^\circ$
$\theta_{23} = 42.8 \begin{smallmatrix} +4.7 \\ -2.9 \end{smallmatrix} \left( \begin{smallmatrix} +10.7 \\ -7.3 \end{smallmatrix} \right)^\circ$	Same
$\theta_{13} = 5.6 \begin{smallmatrix} +3.0 \\ -2.7 \end{smallmatrix} (\leq 12.5)^\circ$	$5.1 \begin{smallmatrix} +3.0 \\ -3.3 \end{smallmatrix} (\leq 12.0)^\circ$
$[\sin^2 \theta_{13} = 0.0095 \begin{smallmatrix} +0.013 \\ -0.007 \end{smallmatrix} (\leq 0.047)]$	$[0.008 \begin{smallmatrix} +0.012 \\ -0.007 \end{smallmatrix} (\leq 0.043)]$
$\delta_{\text{CP}} \in [0, 360]$	Same

For each parameter the ranges are obtained after marginalizing with respect to the other parameters. For  $\Delta m_{31}^2$  the allowed ranges are formed by two disconnected intervals which correspond to the two possible mass orderings. The absolute best-fit lays in the positive  $\Delta m_{31}^2 = +2.46 \times 10^{-3} \text{ eV}^2$ . The  $1\sigma$  and  $3\sigma$  ranges are defined with respect to this absolute minimum. In particular the local best-fit in the inverse mass ordering,  $\Delta m_{31}^2 = -2.36 \times 10^{-3} \text{ eV}^2$ , is at a  $\Delta\chi^2 = 0.12$ .

In summary we have presented the results of an up-to-date global analysis of neutrino oscillation data including the detailed analysis of the Borexino spectra, the lower value of Ga rate as lastly measured in SAGE, the low energy threshold analysis of the combined SNO phase I and phase II, the results for  $\nu_e$  appearance from MINOS and the recent reanalysis of SK(I+II+III) atmospheric data. We have studied the robustness of the hints of a non-vanishing value of  $\theta_{13}$  under the inclusion of the new data and variations of the assumptions about the solar model and the possible modification of the cross-section for neutrino capture in Ga as advocated by the SAGE collaboration in order to explain their new calibration data.

We found that the inclusion of the new solar data, and in particular of the SNO-LETA results tends to lower the statistical significance of  $\theta_{13} \neq 0$  while the results from  $\nu_e$  appearance from MINOS and the new SK(I+II+III) atmospheric neutrino reanalysis increases it. We conclude that the significance of  $\theta_{13} \neq 0$  is:

	GS98 with Gallium cross-section from [24]	AGSS09 with modified Gallium cross-section [16]
solar+KamLAND	CL = 79% (1.26 $\sigma$ )	CL = 70% (1.05 $\sigma$ )
+ SK(I+II+III) + CHOOZ + LBL(Dis+App)	CL = 81% (1.31 $\sigma$ )	CL = 76% (1.17 $\sigma$ )

The determination of the other oscillation parameters is rather robust.

## Acknowledgments

This work is supported by Spanish MICINN grants 2007-66665-C02-01, FPA-2009-08958 and FPA-2009-09017 and consolider-ingenio 2010 grant CSD-2008-0037, by CSIC grant 200950I111, by CUR Generalitat de Catalunya grant 2009SGR502, by Comunidad Autonoma de Madrid through the HEPHACOS project S2009/ESP-1473, by USA-NSF grant PHY-0653342 and by EU grant EURONU.

## References

- [1] B. Pontecorvo, *Neutrino experiments and the question of leptonic-charge conservation*, *Sov. Phys. JETP* **26** (1968) 984–988.
- [2] V. N. Gribov and B. Pontecorvo, *Neutrino astronomy and lepton charge*, *Phys. Lett.* **B28** (1969) 493.
- [3] M. C. Gonzalez-Garcia and M. Maltoni, *Phenomenology with Massive Neutrinos*, *Phys. Rept.* **460** (2008) 1–129, [[arXiv:0704.1800](#)].
- [4] Z. Maki, M. Nakagawa, and S. Sakata, *Remarks on the unified model of elementary particles*, *Prog. Theor. Phys.* **28** (1962) 870–880.
- [5] M. Kobayashi and T. Maskawa, *CP Violation in the Renormalizable Theory of Weak Interaction*, *Prog. Theor. Phys.* **49** (1973) 652–657.
- [6] S. M. Bilenky, J. Hosek, and S. T. Petcov, *On Oscillations of Neutrinos with Dirac and Majorana Masses*, *Phys. Lett.* **B94** (1980) 495.
- [7] P. Langacker, S. T. Petcov, G. Steigman, and S. Toshev, *On the Mikheev-Smirnov-Wolfenstein (MSW) Mechanism of Amplification of Neutrino Oscillations in Matter*, *Nucl. Phys.* **B282** (1987) 589.
- [8] G. L. Fogli, E. Lisi, A. Marrone, A. Palazzo, and A. M. Rotunno, *Neutrino masses and mixing: 2008 status*, *Nucl. Phys. Proc. Suppl.* **188** (2009) 27–30.
- [9] T. Schwetz, M. A. Tortola, and J. W. F. Valle, *Three-flavour neutrino oscillation update*, *New J. Phys.* **10** (2008) 113011, [[arXiv:0808.2016](#)].
- [10] M. Maltoni and T. Schwetz, *Three-flavour neutrino oscillation update and comments on possible hints for a non-zero  $\theta_{13}$* , [arXiv:0812.3161](#).
- [11] G. L. Fogli, E. Lisi, A. Marrone, A. Palazzo, and A. M. Rotunno, *Hints of  $\theta_{13} > 0$  from global neutrino data analysis*, *Phys. Rev. Lett.* **101** (2008) 141801, [[arXiv:0806.2649](#)].
- [12] G. L. Fogli, E. Lisi, A. Marrone, A. Palazzo, and A. M. Rotunno, *SNO, KamLAND and neutrino oscillations:  $\theta_{13}$* , [arXiv:0905.3549](#).
- [13] B. T. Cleveland *et al.*, *Measurement of the solar electron neutrino flux with the Homestake chlorine detector*, *Astrophys. J.* **496** (1998) 505–526.
- [14] F. Kaether, W. Hampel, G. Heusser, J. Kiko, and T. Kirsten, *Reanalysis of the GALLEX solar neutrino flux and source experiments*, [arXiv:1001.2731](#).
- [15] R. L. Hahn, *Radiochemical solar neutrino experiments, 'successful and otherwise'*, *J. Phys. Conf. Ser.* **136** (2008) 022003.

- [16] **SAGE** Collaboration, J. N. Abdurashitov *et al.*, *Measurement of the solar neutrino capture rate with gallium metal. III: Results for the 2002–2007 data-taking period*, *Phys. Rev.* **C80** (2009) 015807, [[arXiv:0901.2200](#)].
- [17] **Super-Kamioke** Collaboration, J. Hosaka *et al.*, *Solar neutrino measurements in Super-Kamiokande-I*, *Phys. Rev.* **D73** (2006) 112001, [[hep-ex/0508053](#)].
- [18] **SNO** Collaboration, B. Aharmim *et al.*, *Measurement of the  $\nu_e$  and total B-8 solar neutrino fluxes with the Sudbury Neutrino Observatory phase I data set*, *Phys. Rev.* **C75** (2007) 045502, [[nucl-ex/0610020](#)].
- [19] **SNO** Collaboration, B. Aharmim *et al.*, *Electron energy spectra, fluxes, and day-night asymmetries of B-8 solar neutrinos from the 391-day salt phase SNO data set*, *Phys. Rev.* **C72** (2005) 055502, [[nucl-ex/0502021](#)].
- [20] **SNO** Collaboration, B. Aharmim *et al.*, *An Independent Measurement of the Total Active 8B Solar Neutrino Flux Using an Array of  $^3\text{He}$  Proportional Counters at the Sudbury Neutrino Observatory*, *Phys. Rev. Lett.* **101** (2008) 111301, [[arXiv:0806.0989](#)].
- [21] **SNO** Collaboration, B. Aharmim *et al.*, *Low Energy Threshold Analysis of the Phase I and Phase II Data Sets of the Sudbury Neutrino Observatory*, [arXiv:0910.2984](#).
- [22] **Borexino** Collaboration, C. Arpesella *et al.*, *Direct Measurement of the Be-7 Solar Neutrino Flux with 192 Days of Borexino Data*, *Phys. Rev. Lett.* **101** (2008) 091302, [[arXiv:0805.3843](#)].
- [23] **Borexino** Collaboration, G. Bellini *et al.*, *Measurement of the solar 8B neutrino flux with 246 live days of Borexino and observation of the MSW vacuum-matter transition*, [arXiv:0808.2868](#).
- [24] J. N. Bahcall, *Gallium solar neutrino experiments: Absorption cross sections, neutrino spectra, and predicted event rates*, *Phys. Rev.* **C56** (1997) 3391–3409, [[hep-ph/9710491](#)].
- [25] M. C. Gonzalez-Garcia, M. Maltoni, and J. Salvado, *Direct determination of the solar neutrino fluxes from solar neutrino data*, [arXiv:0910.4584](#).
- [26] L. Wolfenstein, *Neutrino oscillations in matter*, *Phys. Rev.* **D17** (1978) 2369–2374.
- [27] S. P. Mikheev and A. Y. Smirnov, *Resonance enhancement of oscillations in matter and solar neutrino spectroscopy*, *Sov. J. Nucl. Phys.* **42** (1985) 913–917.
- [28] M. Asplund, N. Grevesse, and J. Sauval, *The solar chemical composition*, *ASP Conference Series* **336** (2005) 25.
- [29] M. Asplund, N. Grevesse, A. J. Sauval, and P. Scott, *The chemical composition of the Sun*, *Ann. Rev. Astron. Astrophys.* **47** (2009) 481–522, [[arXiv:0909.0948](#)].
- [30] N. Grevesse and A. J. Sauval, *Standard Solar Composition*, *Space Sci. Rev.* **85** (1998) 161–174.
- [31] J. N. Bahcall, S. Basu, M. Pinsonneault, and A. M. Serenelli, *Helioseismological Implications of Recent Solar Abundance Determinations*, *Astrophys. J.* **618** (2005) 1049–1056, [[astro-ph/0407060](#)].
- [32] W. J. Chaplin *et al.*, *Solar heavy element abundance: constraints from frequency separation ratios of low-degree p modes*, *Astrophys. J.* **670** (2007) 872–884, [[arXiv:0705.3154](#)].

- [33] S. Basu *et al.*, *Solar abundances and helioseismology: fine structure spacings and separation ratios of low-degree  $p$  modes*, *Astrophys. J.* **655** (2007) 660–671, [[astro-ph/0610052](#)].
- [34] J. N. Bahcall, A. M. Serenelli, and S. Basu, *New solar opacities, abundances, helioseismology, and neutrino fluxes*, *Astrophys. J.* **621** (2005) L85–L88, [[astro-ph/0412440](#)].
- [35] A. Serenelli, S. Basu, J. W. Ferguson, and M. Asplund, *New Solar Composition: The Problem With Solar Models Revisited*, [arXiv:0909.2668](#).
- [36] S. Goswami and A. Y. Smirnov, *Solar neutrinos and 1-3 leptonic mixing*, *Phys. Rev.* **D72** (2005) 053011, [[hep-ph/0411359](#)].
- [37] **KamLAND** Collaboration, I. Shimizu, *KamLAND (anti-neutrino status)*, *J. Phys. Conf. Ser.* **120** (2008) 052022.
- [38] A. B. Balantekin and D. Yilmaz, *Contrasting solar and reactor neutrinos with a non-zero value of  $\theta_{13}$* , *J. Phys.* **G35** (2008) 075007, [[arXiv:0804.3345](#)].
- [39] **Super-Kamiokande** Collaboration, Y. Ashie *et al.*, *A Measurement of Atmospheric Neutrino Oscillation Parameters by Super-Kamiokande I*, *Phys. Rev.* **D71** (2005) 112005, [[hep-ex/0501064](#)].
- [40] P. Litchfield, “Review of atmospheric  $\nu$  data.” Talk given at the *XXII International Conference on Neutrino Physics*, Santa Fe, New Mexico, June 13–19, 2006.
- [41] **Kamiokande** Collaboration, S.-. R. Wendell *et al.*, *Atmospheric neutrino oscillation analysis with sub-leading effects in Super-Kamiokande I, II, and III*, [arXiv:1002.3471](#).
- [42] **K2K** Collaboration, M. H. Ahn *et al.*, *Measurement of Neutrino Oscillation by the K2K Experiment*, *Phys. Rev.* **D74** (2006) 072003, [[hep-ex/0606032](#)].
- [43] **MINOS** Collaboration, P. Adamson *et al.*, *Measurement of Neutrino Oscillations with the MINOS Detectors in the NuMI Beam*, *Phys. Rev. Lett.* **101** (2008) 131802, [[arXiv:0806.2237](#)].
- [44] R. Patterson, “New results for  $\nu_\mu \rightarrow \nu_e$  oscillations in MINOS.” Talk presented at the Fermilab National Accelerator Laboratory, April 9, 2010.
- [45] G. Pawloski, “New results for  $\nu_\mu \rightarrow \nu_e$  oscillations in the MINOS experiment.” Talk presented at the SLAC National Accelerator Laboratory, April 9, 2010.
- [46] **CHOOZ** Collaboration, M. Apollonio *et al.*, *Limits on Neutrino Oscillations from the CHOOZ Experiment*, *Phys. Lett.* **B466** (1999) 415–430, [[hep-ex/9907037](#)].
- [47] **MINOS** Collaboration, P. Adamson *et al.*, *Search for muon-neutrino to electron-neutrino transitions in MINOS*, *Phys. Rev. Lett.* **103** (2009) 261802, [[arXiv:0909.4996](#)].